European Journal of Radiology Open 12 (2024) 100563

Contents lists available at ScienceDirect

European Journal of Radiology Open

journal homepage: www.elsevier.com/locate/ejro

Narrow band imaging-based radiogenomics for predicting radiosensitivity in nasopharyngeal carcinoma

Cheng-Wei Tie [a], Xin Dong [b], Ji-Qing Zhu [a], Kai Wang [c], Xu-Dong Liu [a], Yu-Meng Liu [a], Gui-Qi Wang [a], Ye Zhang [c,*], Xiao-Guang Ni [a,*]

[a] Department of Endoscopy, National Cancer Center/National Clinical Research Center for Cancer/Cancer Hospital, Chinese Academy of Medical Sciences and Peking Union Medical College, Beijing, China
[b] Department of Clinical Laboratory, National Cancer Center/National Clinical Research Center for Cancer/Cancer Hospital, Chinese Academy of Medical Sciences and Peking Union Medical College, Beijing, China
[c] Department of Radiotherapy, National Cancer Center/National Clinical Research Center for Cancer/Cancer Hospital, Chinese Academy of Medical Sciences and Peking Union Medical College, Beijing, China

HIGHLIGHTS

- NBI performance scores were significantly correlated with the early treatment responses in NPC.
- NBI-based radiomics models provide a new method for predicting radiosensitivity of NPC.
- Radiogenomics shows macrophages affect NPC treatment responses by regulating genes like CCL8, SLC11A1, PTGS2.

ARTICLE INFO

Keywords:
Nasopharyngeal carcinoma
Radiosensitivity
Narrow band imaging
Radiomics
Tumor immune microenvironment

ABSTRACT

Objectives: This study aims to assess the efficacy of narrow band imaging (NBI) endoscopy in utilizing radiomics for predicting radiosensitivity in nasopharyngeal carcinoma (NPC), and to explore the associated molecular mechanisms.

Materials: The study included 57 NPC patients who were pathologically diagnosed and underwent RNA sequencing. They were categorized into complete response (CR) and partial response (PR) groups after receiving radical concurrent chemoradiotherapy. We analyzed 267 NBI images using ResNet50 for feature extraction, obtaining 2048 radiomic features per image. Using Python for deep learning and least absolute shrinkage and selection operator for feature selection, we identified differentially expressed genes associated with radiomic features. Subsequently, we conducted enrichment analysis on these genes and validated their roles in the tumor immune microenvironment through single-cell RNA sequencing.

Results: After feature selection, 54 radiomic features were obtained. The machine learning algorithm constructed from these features showed that the random forest algorithm had the highest average accuracy rate of 0.909 and an area under the curve of 0.961. Correlation analysis identified 30 differential genes most closely associated with the radiomic features. Enrichment and immune infiltration analysis indicated that tumor-associated macrophages are closely related to treatment responses. Three key NBI differentially expressed immune genes (NBI-DEIGs), namely CCL8, SLC11A1, and PTGS2, were identified as regulators influencing treatment responses through macrophages.

Conclusion: NBI-based radiomics models introduce a novel and effective method for predicting radiosensitivity in NPC. The molecular mechanisms may involve the functional states of macrophages, as reflected by key regulatory genes.

Abbreviations: NBI, narrow band imaging; NPC, nasopharyngeal carcinoma; NBI-DEIGs, NBI-differentially expressed immune genes; WLI, white light imaging; ScRNA-seq, single-cell RNA sequencing; TAMs, tumor-associated macrophages.

* Corresponding authors.
E-mail addresses: drzye1983@163.com (Y. Zhang), nixiaoguang@126.com (X.-G. Ni).

https://doi.org/10.1016/j.ejro.2024.100563
Received 18 November 2023; Received in revised form 1 April 2024; Accepted 15 April 2024

1. Introduction

Nasopharyngeal carcinoma (NPC) arises from the epithelial lining of the nasopharynx and has a particularly high prevalence in Southern China, Southeast Asia and North Africa [1]. Intensity-modulated radiotherapy (IMRT) is the primary NPC treatment method because of the sensitivity of NPC to radiotherapy [2]. Presently, the radical prescription dose in the target area of nasopharyngeal radiotherapy is approximately 70 Gy, and individuals with the same TNM stage are essentially prescribed the same treatment plan. Although achieving short-term excellent therapeutic effects, this dose prescription lacks individualized consideration. Radioresistant patients may have insufficient doses, however, radiosensitive patients may have severe normal tissue damage. The question of how to predict radiosensitivity before radiotherapy and give individualized radiotherapy doses to achieve a better curative effect and less therapeutic damage is an urgent clinical problem in NPC treatment [3].

Currently, diagnostic and prognostic imaging tools for NPC include computed tomography (CT), magnetic resonance imaging (MRI), positron emission tomography (PET)-CT, and PET-MRI. While these technologies are crucial for target delineation, treatment planning, dose assessment, and outcome prediction, they fall short in predicting radiosensitivity [4]. Although these technologies are crucial for target delineation, treatment planning, dose assessment, and efficacy prediction, they fall short in predicting radiosensitivity [5–7]. MRI leverages radiomics to transform the physiological information of tumor density into texture features, offering substantial aid and predictive power for the treatment of NPC[6,7]. However, MRI-based radiomics also faces challenges, such as the overly simplistic nature of the features it provides and the lack of widespread availability in primary care hospitals due to the high cost of MRI.

Nasopharyngoscopy, which allows for direct visualization of the nasopharyngeal mucosa, is key to NPC diagnosis and is further enhanced by biopsy for pathological confirmation. Narrow band imaging (NBI) is an advanced endoscopic technique that improves the early detection and diagnostic accuracy of head and neck cancers by revealing mucosal microvascular structures [8]. Our previous research identified unique and patient-specific serpentine microvessels on the surface of the nasopharyngeal mucosa under NBI, which have been shown to strongly correlate with certain tumor microenvironment molecular markers [9]. These markers, in turn, have a direct impact on the prognosis and treatment sensitivity of NPC [10]. Therefore, these tumor surface microvessels may serve as indicators for radiation response in NPC. The present study aims to employ radiogenomics to extract features from NBI images and combine them with RNA sequencing analysis. Our objective is to decipher the predictive capability and potential molecular mechanisms of these microvessels in determining the radiotherapy response in NPC.

2. Materials and methods

2.1. Patients

From January 2013 to December 2016, we initially prospectively enrolled 67 newly diagnosed NPC patients from the Cancer Hospital of the Chinese Academy of Medical Sciences for chemoradiotherapy. Eligibility criteria included: (1) histological confirmation of NPC, (2) no prior anti-tumor treatments before baseline MRI, (3) absence of distant metastasis, (4) pre-treatment nasopharynx MRI and nasopharyngoscopy, (5) radical cisplatin-based chemoradiotherapy, and (6) tumor tissues subjected to RNA sequencing analysis. Patients were excluded if they: (1) had a history of other cancers, (2) presented MRI contraindications, and (3) No complete medical records. Tumor staging was determined based on the 8th edition of the AJCC system. Our study received approval from the hospital's Medical Ethics Committee (NO. NCC2014G-01) [8], and all participants provided written informed consent.

2.2. Patient treatment and early response evaluation of CCRT

Patients enrolled in the study received standard concurrent chemoradiotherapy (CCRT) at our hospital. IMRT was administered using a 6 MV X-ray linear accelerator at 2.12–2.24 Gy/f over 33 fractions, resluting in a total dose between 69.96 and 73.92 Gy to the gross tumor volume (GTV). High risk and low risk clinical tumor volume (CTV) were received by 60.06 and 50.96 Gy in 33 fractions and 28 fractions with 1.82 Gy/f. Chemotherapy involved two cycles of cisplatin, delivered intravenously at 100 mg/m^2 on the first day of each 21-day cycle. Two MRI scans were taken for each patient: (1) pre-treatment, 0–5 days between the first MRI examination and the start of treatment; (2) post-treatment, 0–3 days from the end of radiotherapy. Post-CCRT, patients were sorted into two groups: complete response (CR) or partial response (PR) groups, following the RECIST 1.1 guidelines [11]. Regular follow-ups were scheduled: quarterly for the first two years, biannually for years 3–5, and yearly afterwards.

2.3. Pretreatment NBI performance score

The Olympus Evis Lucera 260 system, equipped with a BF-260 videobronchoscope (Olympus Medical Systems, Tokyo, Japan), was used to inspect the nasopharyngolarynx. Both white light imaging (WLI) and NBI modes captured representative images prior to radiotherapy. For the NBI assessment of new microvessels on the NPC tissue surface, the grading was as follows: the microvessels appearing on the tumor surface accounted for < 25 % of the whole tumor surface as grade 1, 25–50 % as grade 2, 50–75 % as grade 3, and > 75 % as grade 4. Three senior endoscopists scored the NBI performance of each case, and the final score was agreed by the three after consultation.

2.4. RNA extraction and transcriptome sequencing

Before treatment, all patients were subjected to NBI endoscopy and biopsy. Part of the biopsy tissue was sent for pathology, while the remainder underwent RNA sequencing. Initial tumor samples from NPC patients were stored at −80 ℃. RNA was extracted from these frozen samples with TRIzol (Invitrogen, Carlsbad, CA, USA) as per the provided guidelines. The RNA's quality was then validated using an Agilent 2100 Bioanalyzer (Agilent Technologies, Palo Alto, CA, USA) and all passed the QC benchmark (RIN>7). The raw sequencing data for these patients is accessible in the Genome Sequence Archive (https://bigd.big.ac.cn/gsa) under the identifier HRA000790.

2.5. Region of interest segmentation of nasopharyngeal images under NBI mode

Two senior doctors, each boasting over a decade of experience, delineated the region of interest (ROI) on NBI images. When discrepancies in the ROI appeared in the images, they collaboratively reviewed and re-marked them using the ITK-SNAP software (version 3.8.0). To assess the consistency in radiomics feature extraction, intraclass correlation coefficients (ICCs) were employed. These two doctors independently examined features from a selection of 30 random patients, ensuring a repeatability check for ROI-based radiomics. Features showcasing an ICC value greater than 0.75, indicating superior stability, were taken into account. While these doctors weren't privy to the patients' clinical or pathological information, they were informed of the patients' NPC diagnosis. Subsequently, to ensure the robustness and generalizability of the radiomics model for predicting treatment outcomes in NPC, we adopted a random allocation method to divide NBI images into different groups. This method involved using a random number generator to assign each image to one of two groups. Specifically, images were randomly allocated to either the training or test

group, based on a stratified proportion according to radiosensitivity, using a 4:1 ratio.

2.6. Radiomics feature extraction and selection

The residual network 50 (ResNet50) architecture was adopted to develop deep convolutional neural networks (CNNs) for deep learning feature extraction, extracting 2048 features. To avoid overfitting, a rigorous approach was undertaken for Feature Reduction and Selection: Initially, to reduce the dimensionality of our feature space, we applied a more stringent feature selection process. Using least absolute shrinkage and selection operator (LASSO), we were able to identify and retain only the most informative features, thereby reducing the complexity of our model. All feature lines were standardized by the z-score standardization method, and the correlation between features was calculated by the Spearman correlation coefficient. One of the two features was retained for features with a correlation coefficient > 0.4.

Then, the LASSO logistic regression algorithm, with penalty parameter tuning conducted by 10-fold cross-validation, was applied to select features with nonzero coefficients from the training cohort. This was complemented by Cross-Validation: We employed k-fold cross-validation during the model training phase to ensure that our model's performance was robust and not overly tailored to a specific subset of the data. This technique also helped us to estimate the model's performance on independent datasets more accurately.

Regularization Techniques were also incorporated to further prevent overfitting. Techniques such as Lasso regression were included in our model training process. These techniques penalize large coefficients, thus simplifying the model and making it less prone to overfitting.

Test group was conducted by testing our model on an external dataset not used during the model training phase. This step was crucial in assessing the model's generalizability and confirming that the performance metrics obtained during training were consistent when applied to new, unseen data. Deep learning feature extraction and machine learning modeling are based on Python (version: 3.9.5). Accuracy, area under the mean receiver operating characteristic curve (AUC), confusion matrix, sensitivity, and specificity were used as metrics to evaluate model performance and goodness of fit.

2.7. Differential expression analysis of NBI-associated immune genes

We referenced the list of immune-related genes from the ImmPort database to identify immune genes in our dataset. We then correlated these genes with the NBI deep learning features (criteria: $r > 0.5$, $P < 0.05$). The identified NBI-associated immune genes underwent differential expression assessment through three statistical tools: DESeq2, edgeR, and limma-Voom. These analyses yielded NBI-Differentially Expressed Immune Genes (NBI-DEIGs). Subsequently, we applied the GO enrichment and KEGG pathway analyses on the NBI-DEIGs utilizing the R package 'clusterProfiler', with visual enhancements made via GOplot and tinyarray R packages.

2.8. Analysis of tumor-infiltrating immune cells

Initially, using the ESTIMATE algorithm, we evaluated the tumor purity, ESTIMATE score, immune score, and stromal score of our NPC samples based on their RNA sequencing data with the ESTIMATE R package. Following this, we employed ssGSEA via the GSVA R package to gauge the presence of 28 immune cell subtypes from the gene expression data. We then derived the ssGSEA scores for each immune cell in the NPC samples and assessed differences in radiosensitivity among them with the Wilcoxon test using the ggpubr R package. The defining gene panels for each immune cell type were referenced from a recent study [12].

2.9. Single-cell RNA sequencing and data analysis

We accessed scRNA-seq data of 15 NPC tumors from Chen et al.'s study via the CNGB nucleotide sequence archive [13]. Using the Seurat R package (version 4.2.0), we converted the data and applied quality filters, excluding cells based on gene expression criteria and mitochondrial gene expression. Dimensionality was reduced using principal component analysis followed by UMAP, and clustering was done using the Seurat package's FindClusters function. We categorized clusters by the average expression of specific gene sets, identifying major cell types like epithelial cells, myeloid cells, T cells, and B cells. Within the myeloid cells, further classification was done into macrophages, monocytes, plasmacytoid dendritic cells, and dendritic cells, based on particular gene expressions.

2.10. Statistical analysis

All statistical analyses were conducted with R statistical software (version 3.5.3). $P < 0.05$ was considered statistically significant.

3. Results

3.1. Patient characteristics and NBI image collection

In our study, 57 NPC patients were analyzed, and they were finally categorized into the CR and PR groups based on their treatment assessments. We gathered a total of 341 NBI images from all the NPC patients. Due to inadequate image quality, 74 of these images were excluded. Thus, 267 NBI images were considered for the subsequent radiomics analysis, comprising 181 images from the CR group and 86 from the PR group (Fig. 1). Analysis of T-stage, N-stage, age, and gender revealed no statistically significant differences between the two groups ($P > 0.05$). The entire patient group had a median follow-up duration of 54 months (Table 1).

3.2. Correlation analysis of pretreatment NBI performance scores with tumor treatment responses and prognosis

For NPC cases, the NBI performance scores, representing the tumor surface microvessels, were collected prior to CCRT. Two representative cases from the CR and PR groups were selected to highlight the stark contrast both in NBI images and in treatment responses (Fig. 2A). The data demonstrated that the CR group predominantly had patients with high NBI scores, while the PR group had those with low NBI scores. There was a notable correlation between NBI scores and early treatment response ($P < 0.001$, $r = 0.87$) (Fig. 2B). Moreover, the disease-free survival (DFS) differed significantly among patients based on their NBI scores, with higher scores pointing to longer DFS ($P = 0.006$) (Fig. 2C).

3.3. Feature selection and optimal machine learning algorithm

In the study, 2048 features from each NBI image were extracted using the ResNet50 architecture. This architecture showed emphasis on vascular dense regions in the CR group and on the tumor overall in the PR group, aligning with clinical judgments (Fig. 3A). After performing a Spearman correlation analysis to remove redundancy, 383 features remained, which was further reduced to 54 using the LASSO classifier. Six machine learning algorithms were tested: support vector machines (SVM), K nearest neighbor (KNN), random forest, ExtraTrees, eXtreme Gradient Boosting (XGBoost), and Light Gradient Boosting Machine (LightGBM). Among them, the random forest algorithm demonstrated the highest average accuracy (0.909) and AUC (0.961) in the test groups, establishing it as the most suitable for building NBI-based radiomics models (Fig. 3B-E; Table 2).

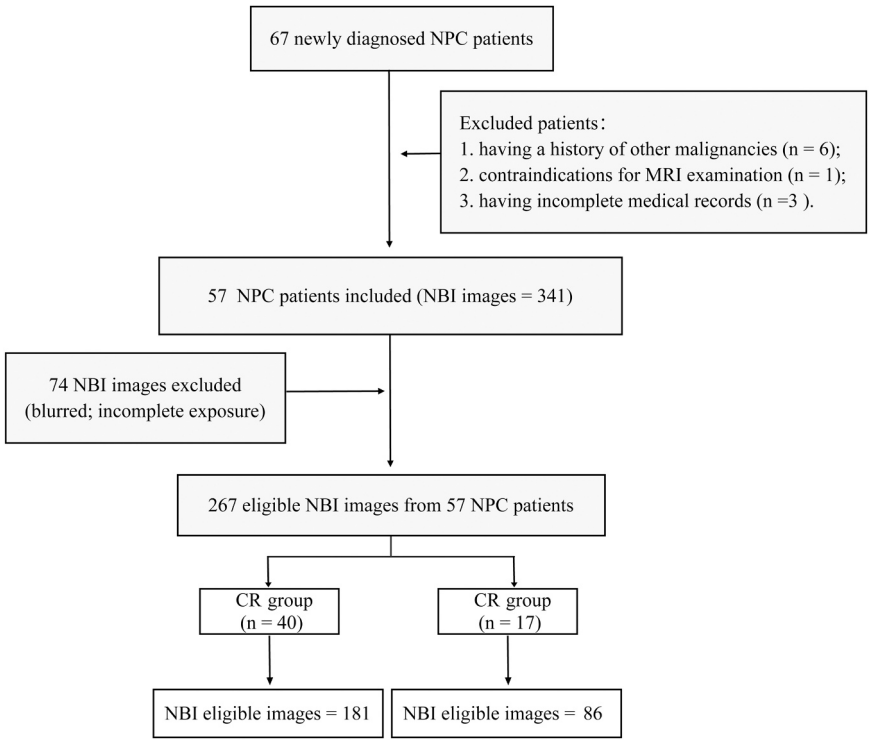

Fig. 1. Schedule of patient enrolment and NBI image collection.

Table 1
Characteristics of the enrolled patients in CR and PR groups.

Clinical characteristics	PR group (n=17)	CR group (n=40)	P value
Age (mean ± SD, years)	41.1 ± 15.9	40.2 ± 18.9	0.86
Gender			0.49
Male	4 (23.5)	13 (32.5)	
Female	13 (76.5)	27 (67.5)	
Histology			0.28
Undifferentiated Non-keratinising	8 (47.1)	25 (62.5)	
Differentiated Non-keratinising	9 (52.9)	15 (37.5)	
T stage			0.25
T1	0 (0)	4 (10)	
T2	4 (23.5)	4 (10)	
T3	5 (29.4)	18 (45)	
T4	8 (47.1)	14 (35)	
N stage			0.13
N1	8 (47.1)	8 (20)	
N2	6 (35.3)	20 (50)	
N3	3 (17.6)	12 (30)	
Overall stage			0.48
II	6 (30)	6 (16.2)	
III	8 (40)	18 (48.6)	
IV	6 (30)	13 (35.2)	
EA-IgA			0.63
positive	2 (11.8)	3 (7.5)	
negative	15 (88.2)	37 (92.5)	
VCA-IgA			0.55
positive	0 (0)	3 (7.5)	
negative	17 (100)	37 (92.5)	
Pretreatment NBI performance scores			< 0.001
1	11 (64.7)	1 (2.5)	
2	4 (23.5)	12 (30)	
3	1 (5.9)	19 (47.5)	
4	1 (5.9)	8 (20)	
Disease-free survival (months)	39.1 ± 21.9	48.6 ± 15.3	0.04

3.4. Differential gene expression analysis

From 2043 immune genes correlated with the 54 deep-learning features of NBI ($r > 0.5$, $P < 0.05$), we analyzed 1094 relevant genes for differences. We identified 14 down-regulated and 16 up-regulated NBI-DEIGs. In terms of GO biological processes (BP), the main enrichment terms were 'mononuclear cell migration', 'response to interferon-gamma', 'positive chemotaxis', 'chemokine-mediated signaling pathway', and 'monocyte chemotaxis' (Fig. 4A). The NBI-DEIGs were notably present in several KEGG pathways. The down-regulated genes primarily appeared in signal transduction pathways like 'TGF-beta signaling' and 'Hippo signaling', whereas up-regulated genes were predominantly in cancer-associated pathways such as 'small cell lung cancer' and 'gastric cancer' (Fig. 4B).

3.5. Analysis of tumor-infiltrating immune cells

To delve deeper into the link between treatment response and immune infiltration in NPC, we analyzed immune cell infiltration in NPC patients. The five most prevalent immune cells were macrophage M1, plasma cells, CD4 positive T cell memory cells, macrophage M2, and CD8 positive T cell Examining the immune infiltration within the CR group revealed higher concentrations of M0, M1, and M2 macrophages, as well as CD4 positive T cell memory cells and CD8 positive T cells, compared to other cells. Statistical analysis highlighted that the CR group had significantly higher infiltration levels of M1 macrophage and follicular helper T-cells than the PR group (supplement Fig. 1). Further, we investigated the association between NBI-DEIGs and specific immune cells. Correlation analysis indicated that memory B cells, activated dendritic cells, M0 macrophages, neutrophils, plasma cells, and follicular helper T cells had the strongest associations with NBI-DEIGs. Immune cells exhibited robust correlations, especially with the chemokine subfamily members and the fibroblast growth factor subfamily (Fig. 5).

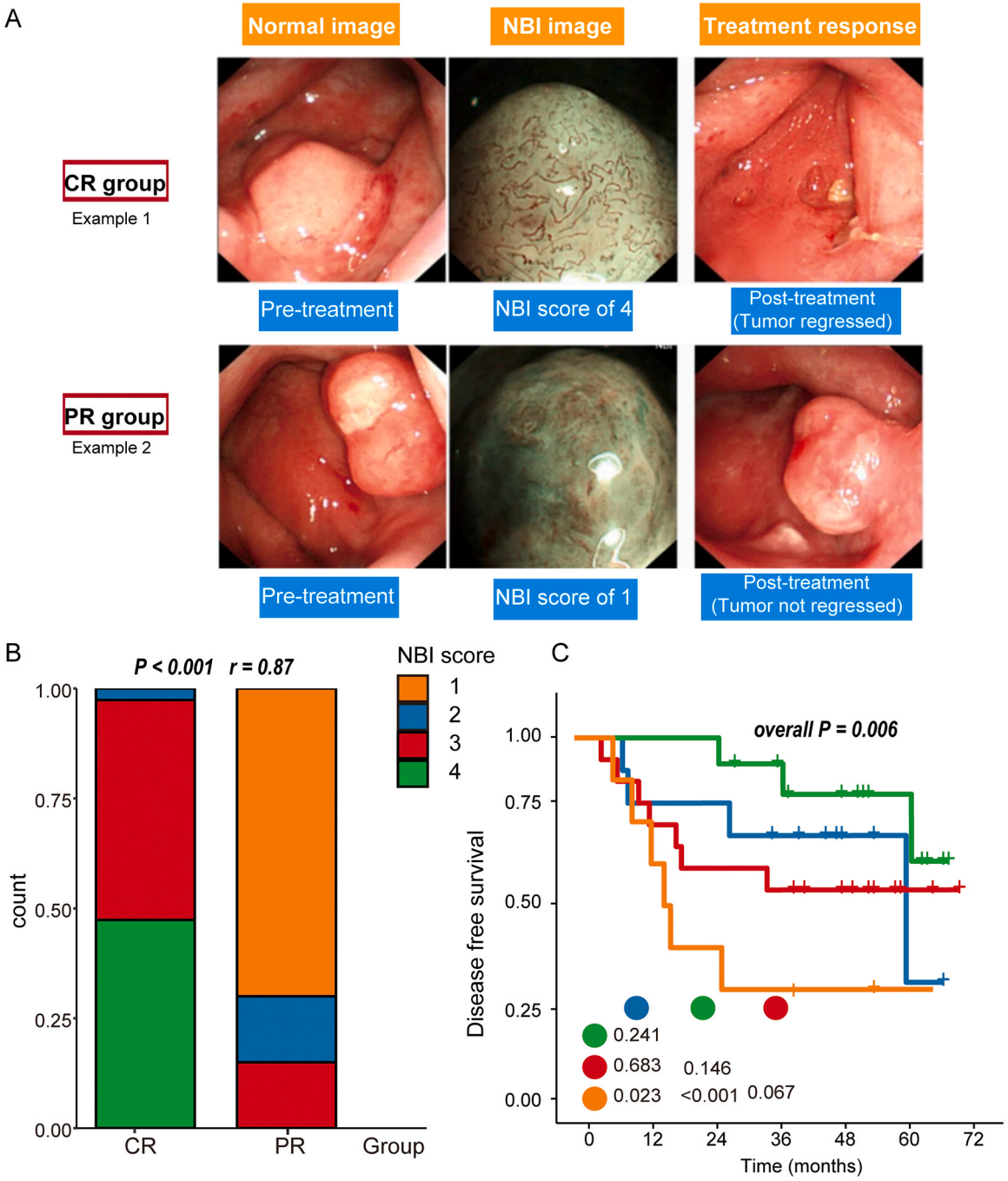

Fig. 2. Pre- and Post-treatment examples in CR and PR groups (A). Positive correlation between NBI performance scores and treatment responses (B). Correlation between disease-free survival (DFS) and NBI performance scores (C).

3.6. Expression and distribution of NBI-DEIGs in the tumor immune microenvironment based on scRNA-seq

From the scRNA-seq profiles, we procured 32,869 single cells. Utilizing a graph-based clustering technique, we categorized these cells into transcriptionally coherent clusters. These clusters were annotated based on the average expression of predefined gene sets, leading us to identify immune (myeloid, T, and B cells) and epithelial cells. Mapping all NBI-DEIGs on UMAP, we highlighted significant genes, notably observing central expression of CCL8, SLC11A1, and PTGS2 with myeloid cells (supplement Fig. 2). Subsequently, we reprocessed the selected 2556 myeloid cells, normalizing, downgrading, and reclustering them. This identified four distinct ssubclusters: monocytes, macrophages, pDCs, and DCs (Fig. 6A-B). Further UMAP mapping of NBI-DEIGs revealed their distribution to be exclusive to the monocytes and macrophages within these subclusters.

4. Discussion

Radiotherapy is the standard radical treatment for NPC. The availability of combined IMRT and chemotherapy has led to a local control rate of over 90 % and a 5-year survival rate of approximately 80 % for patients with NPC [14]. As patients' survival is prolonged, their demand for precise radiotherapy and quality of life becomes increasingly important [15]. Therefore, finding indicators or methods that can easily, economically, and accurately predict radiosensitivity is of great clinical

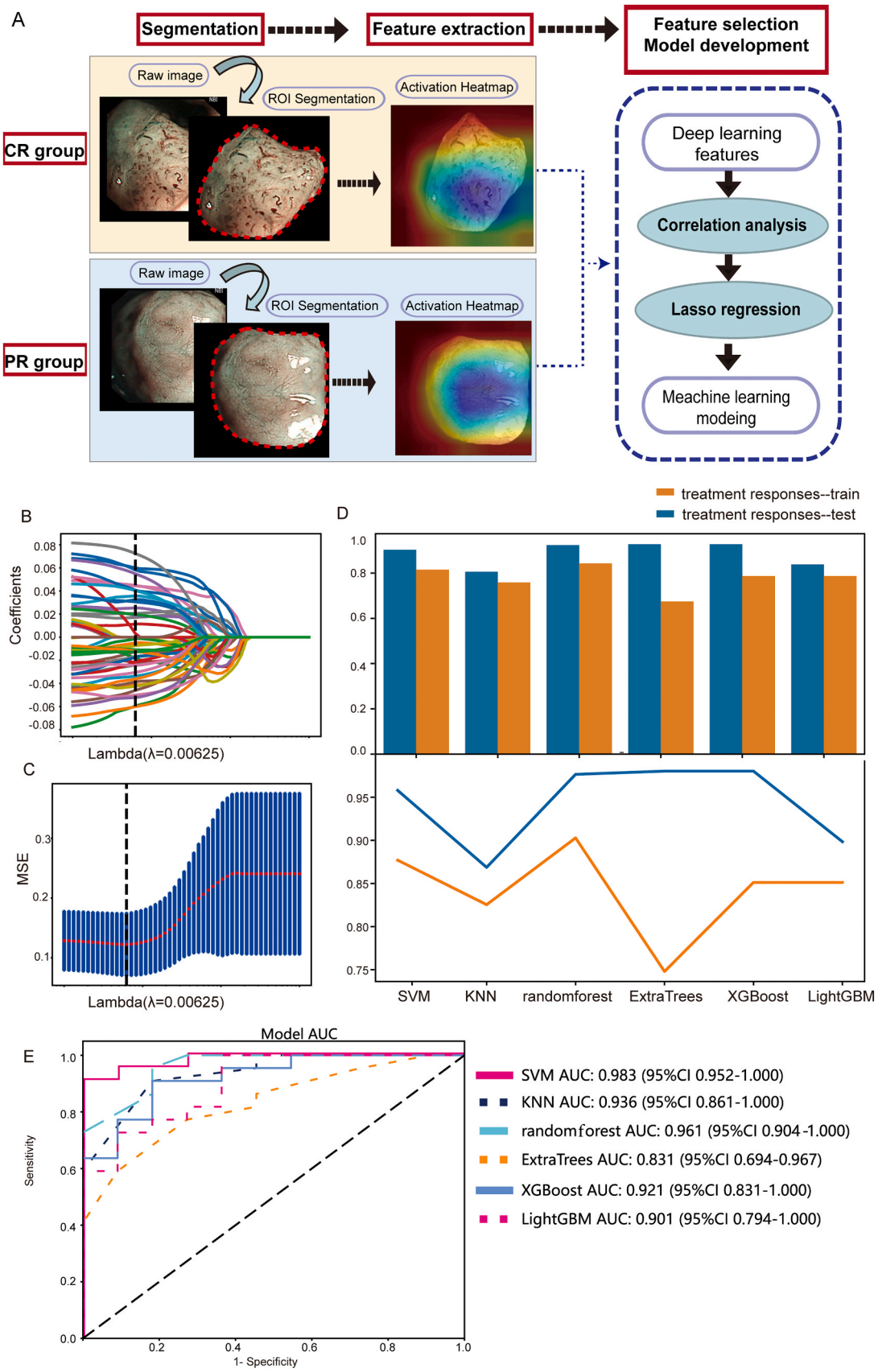

Fig. 3. Feature Selection and Model Evaluation Process. Radiomics analysis flowchart (A). Parameters Screened Based on Minimum Error Mean Value (λmin) (B). Radiomics Features Selected via LASSO Logistic Regression (C). Accuracy Across Different Machine Learning Models (D). Receiver Operating Characteristic (ROC) Curves for Test Group Models (D). LASSO, least absolute shrinkage and selection operator.

Table 2
Differences between machine learning models.

Model name	Set	Accuracy	AUC	95 % CI	Sensitivity	Specificity	Threshold
Random forest	Train	0.995	1	0.994–1	1	0.986	0.6
	Test	0.909	0.961	0.904–1	0.954	0.818	0.6
XGBoost	Train	1	1		1	1	0.793
	Test	0.848	0.921	0.830–1	0.909	0.818	0.706
KNN	Train	0.869	0.963	0.945–0.982	0.762	1	1
	Test	0.818	0.936	0.861–1	0.909	0.818	0.8
SVM	Train	0.974	0.998	0.995–1	1	0.986	0.775
	Test	0.879	0.983	0.952–1	0.909	1	0.81
ExtraTrees	Train	1	1		1	1	1
	Test	0.727	0.831	0.694–0.967	0.591	0.909	0.8
LightGBM	Train	0.903	0.994	0.983–1	0.961	0.986	0.657
	Test	0.848	0.901	0.794–1	0.727	0.909	0.734

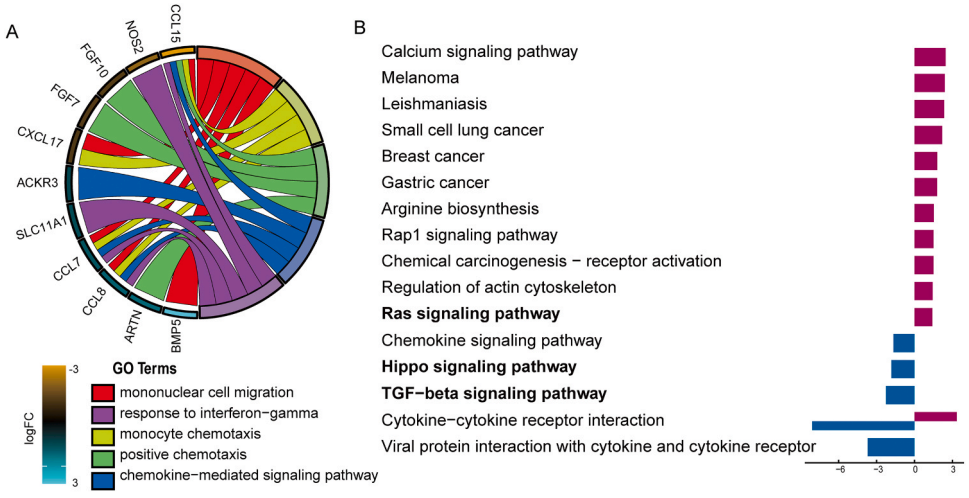

Fig. 4. GO and KEGG enrichment analysis. Cross-examination of GO analyses suggested that a substantial number of genes related to behavior were also enriched in other biological functions such as mononuclear cell migration. Log2 fold changes of gene expression were indicated as colored squares (A). KEGG pathways significantly enriched in CR group are shown in purple; those significantly enriched in the PR group are shown in blue (B).

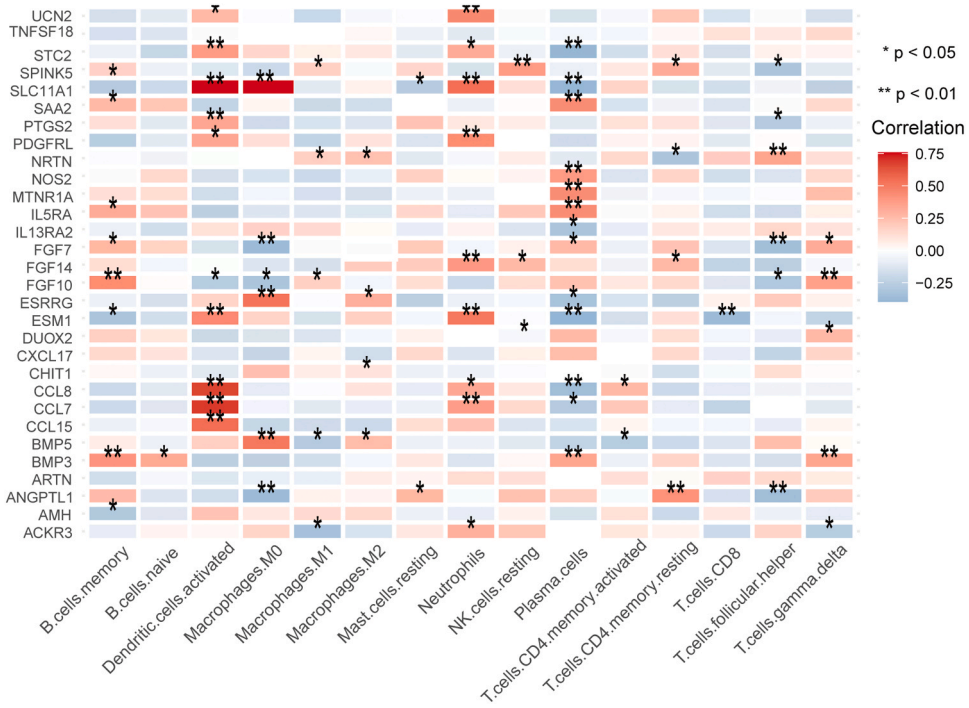

Fig. 5. Correlation analysis of immune cells with NBI-differentially expressed immune genes (NBI-DEIGs).

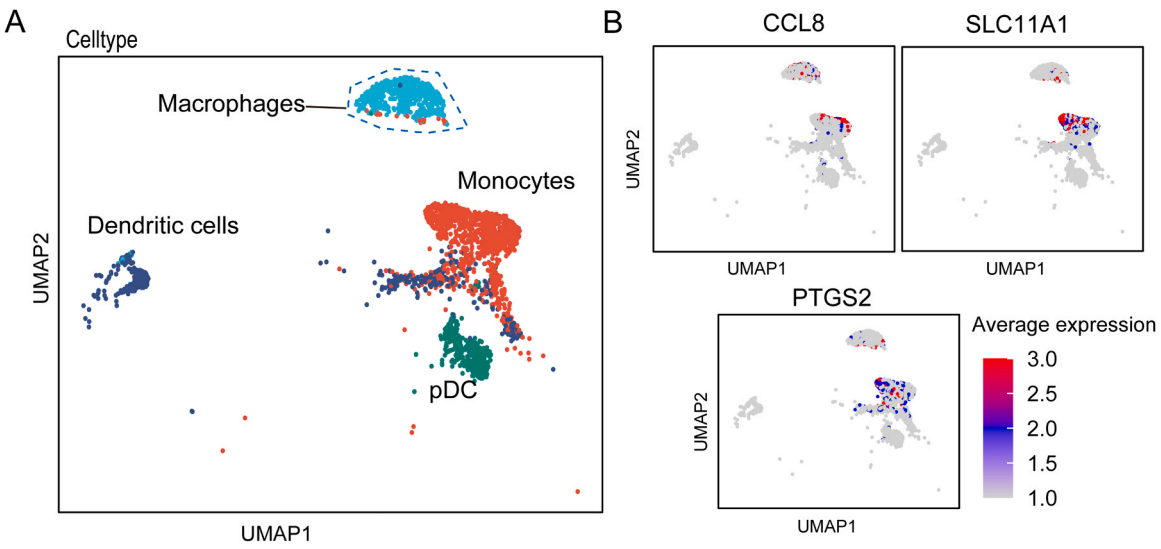

Fig. 6. Validation of the tumor microenvironment of NPC with scRNA-seq. UMAP plots from myeloid cells, each cell is color coded to indicate the relevant cell type (A). Expression and distribution of the 3 NBI-DEIGs (CCL8, SLC11A1, and PTGS2) in NPC myeloid cells (B).

significance in guiding the individualized treatment of NPC patients. Traditional imaging examination is mainly used to detect tumors, diagnose, and make differential diagnosis, compare tumor size and morphological changes before and after treatment, and observe whether the tumor recurred after treatment. However, it is rarely used to evaluate and predict the treatment effect. Currently, imaging techniques have been developed from traditional morphological imaging to functional imaging, which provides a new way to predict the biological behavior of tumor cells. Especially in recent years, the rapid development of radiomics and artificial intelligence technology provides an unprecedented opportunity to improve decision support in oncology in a low-cost and noninvasive way. Radiomic features offer comprehensive and quantitative measurements of tumors including texture, intensity, heterogeneity, and morphology information allowing a comprehensive analysis of tumor phenotype [16]. Recent studies have found that radiomic features may have significantly influenced clinical outcomes and gene expression levels [16]. These features can also be used to develop diagnosis or prognosis models that may serve as a tool for personalized diagnosis and clinical decision support systems [17]. Previous studies have shown that radiomics studies based on CT/MRI/PET-CT could play a predictive role in the treatment response and prognosis of NPC [18–20].

Currently, there are no radiomics studies based on endoscopic images of NPC, which is limited to the recognition of lesion nature by convolutional neural network (CNN) [21], nor are there any studies related to the biological function of tumor cells [22]. NBI is an optical diagnostic technique integrated in endoscopy developed in recent years by filtering the white light source of conventional endoscopy and releasing two wavelengths of light with a central wavelength of 415 nm (blue light) and 540 nm (green light) as the irradiation source. Because the optical properties of hemoglobin are strongly absorbed by blue and green light, the NBI technique increases the contrast and clarity of the mucosal epithelium and microvessels, enabling a more accurate determination of neovascularization and its morphology [23]. NBI endoscopy is easy to set up and operate, and the user can rapidly switch between the conventional WLI and NBI systems by simply pressing a button on the videoendoscope. In this study, we found that the NBI performance score of surface microvessels in NPC was significantly correlated with the radiosensitivity of NPC. Leveraging radiomics, we utilized the deep learning architecture ResNet50 to extract high-dimensional features from NPC imaging datasets. ResNet50's residual learning framework captures intricate tumor microenvironment patterns often missed by traditional imaging [24]. The features extracted span a wide range of radiomic attributes, enriching the tumor's phenotypic profile. Rigorous model validation confirmed its high accuracy in predicting CCRT responses in NPC, further substantiated by external datasets. This integration of deep learning and machine learning not only refines treatment response predictions but also lays the groundwork for personalized NPC treatment strategies, heralding advancements in precision oncology.

To gain a deeper understanding of the interpretability of radiomics based on NBI, we conducted gene sequencing on tumor tissues and analyzed these data from an immunological perspective. Building on previous studies, which have shown that classifying NPC subtypes based on immune profiles in the TME can predict patient survival and response to immunotherapy [25], we identified NBI-DEIGs that are closely associated with NBI features and show significant differences between the CR and PR groups. These genes, closely associated with NBI features, exhibit significant differences between the CR and PR groups, particularly highlighting biological pathways related to TAMs, which are more prevalent in the CR group. Sc-RNA sequencing results confirmed that genes such as CCL8, SLC11A1, and PTGS2 are primarily located in subgroups of monocytes and macrophages, aligning with our bulk sequencing data.

In the TME of NPC, macrophages demonstrate unique characteristics. They appear to be directly recruited, playing a pivotal role in enhancing immune cell infiltration into NPC tissues via chemokine secretion. Notably, a high expression of macrophage traits correlates significantly with improved survival outcomes in NPC patients [26]. Specifically, M1 macrophages are capable of producing substantial amounts of nitric oxide by releasing inducible nitric oxide synthase, which leads to DNA damage and increased sensitivity to radiotherapy [27]. In the CR group, elevated expressions of CCL8 and SLC11A1 might boost therapeutic efficacy by activating M1 macrophages [28]. Conversely, in the PR group, heightened expression of PTGS2 could influence the NF-κB signaling pathway, potentially leading to radiotherapy tolerance [29]. These insights suggest that these genes are crucial in modulating macrophages to affect radiosensitivity.

Furthermore, tumor associated macrophages (TAMs) are known to foster angiogenesis by secreting a range of angiogenic factors, including vascular endothelial growth factor (VEGF), platelet-derived growth factor (PDGF), and transforming growth factor-beta (TGF-β) [30]. Angiogenic factors like thymidine phosphorylase, secreted by TAMs, are instrumental in promoting endothelial cell migration and angiogenesis,

with their expression levels being closely tied to the formation of new blood vessels in tumors [31]. This finding coherently explains the observed variations in NBI image scores among different groups, as NBI imaging reflects the impact of macrophages on tumor vascular surface neovascularization.

However, our study has limitations, including a limited sample size that may affect classification accuracy. Future work should focus on automated lesion segmentation methods and the importance of endoscopist skill in capturing high-quality NBI images. We recognize that selection bias, differences in endoscopic equipment, and variability among endoscopists could have influenced our results. Future research will aim to minimize these biases through standardized protocols, training, and multi-center collaboration to ensure consistency in data collection and analysis. Combining radiological data with clinical risk indicators like EBV antibody levels could further refine classification accuracy.

In summary, our NBI-driven radiomics model establishes a deep connection between NBI features and NPC radiosensitivity. It reveals the intrinsic relationship between tumor microvasculature and the immune environment, offering a simplified yet innovative approach for predicting NPC radiosensitivity. Our comprehensive molecular examination aims to expand our understanding of NBI endoscopy's potential in early treatment response assessment, thereby providing valuable insights for personalized NPC chemoradiotherapy strategies.

Ethical statement

I certify that this manuscript is original and has not been published and will not be submitted elsewhere for publication while being considered by European Journal of Radiology Open. And the study is not split up into several parts to increase the quantity of submissions and submitted to various journals or to one journal over time. No data have been fabricated or manipulated (including images) to support your conclusions. No data, text, or theories by others are presented as if they were our own.

The submission has been received explicitly from all co-authors. And authors whose names appear on the submission have contributed sufficiently to the scientific work and therefore share collective responsibility and accountability for the results.

CRediT authorship contribution statement

Xiao-Guang Ni: Writing – original draft, Resources, Project administration, Data curation. **Ye Zhang:** Writing – review & editing, Writing – original draft, Project administration, Data curation. **Kai Wang:** Validation, Resources. **Ji-Qing Zhu:** Software, Project administration, Methodology. **Xin Dong:** Writing – review & editing, Writing – original draft, Data curation, Conceptualization. **Cheng-Wei Tie:** Writing – review & editing, Writing – original draft, Formal analysis, Data curation, Conceptualization. **Gui-Qi Wang:** Writing – review & editing, Project administration. **Yu-Meng Liu:** Funding acquisition, Formal analysis, Data curation. **Xu-Dong Liu:** Formal analysis, Data curation.

Declaration of Generative AI and AI-assisted technologies in the writing process

Only AI technology was used to improve readability and language.

Declaration of Competing Interest

The authors declare that none of them have any conflicts on interest in relation to the present publication.

Acknowledge

This work was supported by CAMS Innovation Fund for Medical Sciences (CIFMS) (grant number 2022-I2M-C&T-B-059) and Beijing Hope Run Special Fund of Cancer Foundation of China (grant number LC2021A04).

Appendix A. Supporting information

Supplementary data associated with this article can be found in the online version at doi:10.1016/j.ejro.2024.100563.

References

[1] L.L. Tang, W.Q. Chen, W.Q. Xue, et al., Global trends in incidence and mortality of nasopharyngeal carcinoma, Cancer Lett. 374 (2016) 22–30.
[2] K. Wong, E.P. Hui, K.W. Lo, et al., Nasopharyngeal carcinoma: an evolving paradigm, Nat. Rev. Clin. Oncol. 18 (2021) 679–695.
[3] Y.P. Chen, A. Chan, Q.T. Le, et al., Nasopharyngeal carcinoma, Lancet 394 (2019) 64–80.
[4] Y.M. Zhang, G.Z. Gong, Q.T. Qiu, et al., Radiomics for diagnosis and radiotherapy of nasopharyngeal carcinoma, Front. Oncol. 11 (2021) 767134.
[5] Y. Wang, H. Chen, J. Lin, et al., Automatic detection and recognition of nasopharynx gross tumour volume (GTVnx) by deep learning for nasopharyngeal cancer radiotherapy through magnetic resonance imaging, Radiat. Oncol. 18 (2023) 76.
[6] F. Zeng, K.R. Lin, Y.B. Jin, et al., MRI-based radiomics models can improve prognosis prediction for nasopharyngeal carcinoma with neoadjuvant chemotherapy, Magn. Reson. Imaging 88 (2022) 108–115.
[7] X. Ma, X. Chen, J. Li, et al., MRI-only radiotherapy planning for nasopharyngeal carcinoma using deep learning, Front. Oncol. 11 (2021) 713617.
[8] X.G. Ni, G.Q. Wang, The role of narrow band imaging in head and neck cancers, Curr. Oncol. Rep. 18 (2016) 10.
[9] Y. Kumagai, M. Toi, H. Inoue, Dynamism of tumour vasculature in the early phase of cancer progression: outcomes from oesophageal cancer research, Lancet Oncol. 3 (2002) 604–610.
[10] S.L. Chan, B.B. Ma, Novel systemic therapeutic for nasopharyngeal carcinoma, Expert Opin. Ther. Targets 16 (Suppl 1) (2012) S63–S68.
[11] E.A. Eisenhauer, P. Therasse, J. Bogaerts, et al., New response evaluation criteria in solid tumours: revised RECIST guideline (version 1.1), Eur. J. Cancer 45 (2009) 228–247.
[12] P. Charoentong, F. Finotello, M. Angelova, et al., Pan-cancer immunogenomic analyses reveal genotype-immunophenotype relationships and predictors of response to checkpoint blockade, Cell Rep. 18 (2017) 248–262.
[13] Y.P. Chen, J.H. Yin, W.F. Li, et al., Single-cell transcriptomics reveals regulators underlying immune cell diversity and immune subtypes associated with prognosis in nasopharyngeal carcinoma, Cell Res. 30 (2020) 1024–1042.
[14] A.W. Lee, B.B. Ma, W.T. Ng, et al., Management of nasopharyngeal carcinoma: current practice and future perspective, J. Clin. Oncol. 33 (2015) 3356–3364.
[15] Y. Jozaghi, J. Phan, E.Y. Hanna, et al., Functional outcomes and quality of life in patients with sinonasal, nasopharyngeal, and anterior skull base tumors, Curr. Oncol. Rep. 24 (2022) 775–781.
[16] H.J. Aerts, E.R. Velazquez, R.T. Leijenaar, et al., Decoding tumour phenotype by noninvasive imaging using a quantitative radiomics approach, Nat. Commun. 5 (2014) 4006.
[17] W. Duan, B. Xiong, T. Tian, et al., Radiomics in nasopharyngeal carcinoma, Clin. Med. Insights Oncol. 16 (2022) 1363200146.
[18] H. Peng, D. Dong, M.J. Fang, et al., Prognostic value of deep learning PET/CT-based radiomics: potential role for future individual induction chemotherapy in advanced nasopharyngeal carcinoma, Clin. Cancer Res. 25 (2019) 4271–4279.
[19] B. Zhang, J. Tian, D. Dong, et al., Radiomics features of multiparametric MRI as novel prognostic factors in advanced nasopharyngeal carcinoma, Clin. Cancer Res. 23 (2017) 4259–4269.
[20] X. Ming, R.W. Oei, R. Zhai, et al., MRI-based radiomics signature is a quantitative prognostic biomarker for nasopharyngeal carcinoma, Sci. Rep. 9 (2019) 10412.
[21] C. Li, B. Jing, L. Ke, et al., Development and validation of an endoscopic images-based deep learning model for detection with nasopharyngeal malignancies, Cancer Commun. 38 (2018) 59.
[22] W.T. Ng, B. But, H. Choi, et al., Application of artificial intelligence for nasopharyngeal carcinoma management - a systematic review, Cancer Manag. Res. 14 (2022) 339–366.
[23] A. Larghi, P.G. Lecca, G. Costamagna, High-resolution narrow band imaging endoscopy, Gut 57 (2008) 976–986.
[24] M. Beker-Acay, Editorial for "MRI-based deep learning model for distant metastasis-free survival in locoregionally advanced nasopharyngeal Carcinoma, J. Magn. Reson. Imaging 53 (2021) 179–180.
[25] L. Gong, D.L. Kwong, W. Dai, et al., Comprehensive single-cell sequencing reveals the stromal dynamics and tumor-specific characteristics in the microenvironment of nasopharyngeal carcinoma, Nat. Commun. 12 (2021) 1540.
[26] R. Su, L. Cai, P. Xiong, et al., TLR3 expression is a potential prognosis biomarker and shapes the immune-active tumor microenvironment in esophageal squamous cell carcinoma, J. Inflamm. Res. 15 (2022) 1437–1456.
[27] H.H. Baydoun, M.A. Cherian, P. Green, et al., Inducible nitric oxide synthase mediates DNA double strand breaks in Human T-Cell Leukemia Virus Type 1-induced leukemia/lymphoma, Retrovirology 12 (2015) 71.

[28] P. Yang, W. Chen, H. Xu, et al., Correlation of CCL8 expression with immune cell infiltration of skin cutaneous melanoma: potential as a prognostic indicator and therapeutic pathway, Cancer Cell Int. 21 (2021) 635.
[29] C. Tan, L. Liu, X. Liu, et al., Activation of PTGS2/NF-kappaB signaling pathway enhances radiation resistance of glioma, Cancer Med. 8 (2019) 1175–1185.
[30] R. Sumitomo, T. Menju, Y. Shimazu, et al., M2-like tumor-associated macrophages promote epithelial-mesenchymal transition through the transforming growth factor beta/Smad/zinc finger e-box binding homeobox pathway with increased metastatic potential and tumor cell proliferation in lung squamous cell carcinoma, Cancer Sci. 114 (2023) 4521–4534.
[31] F.M. Spinelli, D.L. Vitale, A. Icardi, et al., Hyaluronan preconditioning of monocytes/macrophages affects their angiogenic behavior and regulation of TSG-6 expression in a tumor type-specific manner, FEBS J. 286 (2019) 3433–3449.